Journal of Materials Chemistry A

PAPER

Check for updates

Cite this: J. Mater. Chem. A, 2018, 6, 5452

Crystal structure and compositional effects on the electrical and electrochemical properties of $GdBaCo_{2-x}Mn_xO_{5+\delta}$ ($0 \leq x \leq 2$) oxides for use as air electrodes in solid oxide fuel cells†

Daniel Muñoz-Gil,[a] Esteban Urones-Garrote,[b] Domingo Pérez-Coll,[c] Ulises Amador[d] and Susana García-Martín*[a]

Received 13th December 2017
Accepted 23rd February 2018

DOI: 10.1039/c7ta10923g

rsc.li/materials-a

The effects of the substitution of Co with Mn in the crystal structure, oxygen content, thermal stability and expansion and electrical properties of $GdBaCo_{2-x}Mn_xO_{5+\delta}$ ($0 \leq x \leq 2$) oxides are reported. Composites of $GdBaCo_{2-x}Mn_xO_{5+\delta}$–$Ce_{0.9}Gd_{0.1}O_{2-\delta}$ (70 : 30 wt%) are used as cathode materials and their electrochemical behaviour is presented. Layered-type ordering of Ba and Gd cations in the perovskite structure occurs in the whole system when the materials are prepared in argon but only for compositions in the range corresponding to $x < 1.4$ when the materials are prepared in air. The oxygen content increases with increasing the Mn content, causing thermal stability to improve and thermal expansion to decrease. However, lowering of the dc conductivity and an increase of electrode polarization resistances are observed by Mn substitution for Co. Cation ordering of the Gd and Ba atoms seems to affect the electrochemical properties of the materials.

Introduction

$GdBaCo_2O_{5+\delta}$ is a layered-type perovskite with potential applications as an air-electrode for intermediate temperature solid oxide fuel cells (IT-SOFCs) due to its electrical behavior and high catalytic activity for the oxygen reduction reaction.[1–3] From the point of view of electrical properties, it is a p-type electronic conductor also presenting oxygen-anion conductivity associated with its non-stoichiometric anion sublattice. In this context, layered-type ordering of Gd and Ba in the crystal structure of $GdBaCo_2O_{5+\delta}$ seems to be crucial to the location of anion vacancies within the Gd–O layers, creating very high ion-conducting planes.[4,5] All these aspects contribute to the low electrode polarization resistances measured in symmetrical cells using this oxide as the electrode.[1–3] However, despite the mentioned good qualities, $GdBaCo_2O_{5+\delta}$ shows a substantial number of inconveniences for being used as an air electrode in IT-SOFCs: in addition to the high cost of Co-based materials, this oxide is not thermally stable because it suffers from variation of the oxygen content on heating and presents very high thermal expansion coefficients (TECs) associated with oxygen loss and spin transitions of trivalent cobalt.[6–9]

Substitution of Co with M = Ni, Fe or Cu in the $GdBaCo_{2-x}M_xO_{5+\delta}$ system has proven to increase thermal stability and decrease TECs, though in general, higher electrode polarization resistances are measured in cells fabricated with these electrode-materials.[10–14] In this context, studies of the effects of Mn-doping on the properties of the $GdBaCo_{2-x}Mn_xO_{5+\delta}$ system have not yet been reported, though in the case of $NdBaCo_{2-x}Mn_xO_{5+\delta}$ oxides, good chemical compatibility with $Ce_{0.8}Gd_{0.2}O_{1.90}$ (CGO) and $La_{0.8}Sr_{0.2}Ga_{0.8}Mg_{0.2}O_{2.8}$ (LSGM) electrolytes and low TECs have been determined.[15] However, layered-type ordering of Nd and Ba atoms is only achieved in this system for x values in the range $0 \leq x \leq 1$, unless reducing conditions are used in the synthesis.[15–17] This is because ordering in the A cation-sublattice of the layered-perovskite structure ($AA'B_2O_3$) is not only assisted by differences between the ionic radii and oxidation states of the A and A′ atoms but also depends on the B-type cation, which highly affects the oxygen content too. In fact, although A-cation ordering occurs in Co-based perovskites, ordering in Mn-based perovskites requires a more complicated process and therefore, modification of the properties by A-cation ordering in these materials can be controlled by the preparation method. Thus, layered ordering of Gd and Ba in $GdBaMnFeO_{5+\delta}$ is achieved by using a reducing atmosphere in the first step of the synthesis.[18,19]

[a]Departamento de Química Inorgánica, Facultad de C.C. Químicas, Universidad Complutense, 28040-Madrid, Spain. E-mail: sgmartin@quim.ucm.es

[b]Centro Nacional de Microscopía Electrónica, Universidad Complutense, 28040-Madrid, Spain

[c]Instituto de Cerámica y Vidrio, CSIC, Cantoblanco, 28049 Madrid, Spain

[d]Universidad San Pablo-CEU, CEU Universities, Facultad de Farmacia, Departamento de Química y Bioquímica, Urbanización Montepríncipe, Boadilla del Monte, E-28668, Madrid, Spain

† Electronic supplementary information (ESI) available. See DOI: 10.1039/c7ta10923g

Besides, the improvement of the electrochemical performance of ordered $GdBaMnFeO_{5+\delta}$ oxide as an air electrode in symmetrical cells using CGO as the electrolyte in comparison with the disordered $Gd_{0.5}Ba_{0.5}Mn_{0.5}Fe_{0.5}O_{3-\delta}$ material has been clearly demonstrated.[18] However, $GdBaMnFeO_{5+\delta}$ showed higher electrode polarization resistances in comparison to analogous Co-based phases.[3,12] This feature reinforces the interest in Co-based compositions, which, nevertheless, require further effort to overcome their limitations for practical applications. In addition to the improvements expected both in thermal stability and TECs, substitution of Mn for Co generally extends the redox stability of the material; in this sense, $PrBaMn_2O_{6-\delta}$ has shown high redox stability under reducing conditions and high tolerance to carbon coking and H_2S poisoning, showing good electrochemical performance as an anode not only in SOFCs using hydrocarbon fuels but also in SOECs (solid oxide electrolysis cells).[20,21]

Taking into account all these results and considering that Gd/Ba-compounds seem to present increased oxygen-vacancy concentrations compared to other $REBaCo_2O_{5+\delta}$ layered-perovskites with lower size difference between RE and Ba,[22] which can also enhance the oxygen-anion conductivity, we have studied the influence of the substitution of Co with Mn on the crystal structure and properties of the $GdBaCo_{2-x}Mn_xO_{5+\delta}$ system. We report in this article the influence of preparation conditions on the ordering of Gd and Ba ions in the structure. We also compare the results of the electrode polarization resistances of symmetrical cells using ordered or disordered oxides of the system in the electrodes, finding that layered-type compounds show better electrochemical performance.

Experimental section

$GdBaCo_{2-x}Mn_xO_{5+\delta}$ ($0 \leq x \leq 2$) oxides have been prepared from stoichiometric amounts of Gd_2O_3 (Sigma Aldrich, 99.99%), $BaCO_3$ (Sigma Aldrich, 99.99%), Co_2O_3 (Sigma Aldrich, 99.99%) and Mn_2O_3 (Sigma Aldrich, 99.99%). Gd_2O_3 was heated at 1173 K prior to weighing. These starting compounds were mixed and heated at 1173 K for 12 hours for the decomposition of $BaCO_3$ in air or under a gas flow of argon (purity $\geq$ 99.999). After this first thermal treatment, the samples were re-ground and pelletized and finally heated at 1473 or at 1773 K (those with higher Mn contents) for 48 hours. The thermal treatment was carried out twice with intermediate grinding of all the samples and in two different atmospheres (air and argon). The compounds were quickly cooled to room temperature.

Crystalline phase identification was carried out by powder X-ray diffraction (PXRD) using a PANalytical X'PERT PRO MPD diffractometer with CuKα_1 ($\lambda = 1.5406$ A) radiation and X'PERT PEAPD software. The patterns were taken in step mode with a step size equal to 0.02 (2θ degrees) and time per step equal to 10 s. X-ray diffraction patterns at different temperatures in the 298–1173 K range were taken every 50 K in air after stabilization for 30 min, applying a heating/cooling rate of 2 K min^{-1} on a Multi-Purpose PANalyticalX'Pert PRO MPD diffractometer equipped with an Anton Paar HTK2000 camera.

LeBail fitting (without structural model) of the XRD patterns was performed to obtain the lattice parameters and symmetries (S.G.) of the phases in every sample using Fullprof software.[23,24]

The oxygen content of the compounds was determined by redox titration.[25] A 50 mg sample and an excess of $FeSO_4 \cdot 7H_2O$ (*ca.* 120 to 180 mg) were dissolved in 20 ml of HCl, 75 ml of distilled water and 5 ml of phosphoric acid (the titrations were carried out under an Ar atmosphere for preventing oxidation). As a result, the species (Co and Mn) were reduced to divalent ions and the stoichiometric amount of trivalent iron was formed. The rest of the Fe^{2+} was titrated with a 5×10^{-3} M solution of $K_2Cr_2O_7$ (*ca.* 12–22 ml is required). Two drops of a 0.01 M solution of tris(5,6-dimethyl-1,10-phenanthroline) iron(II) sulfate were used as the indicator; the end-point was detected visually as the colour of the solution changes from red to yellow-green. Thermogravimetric analyses (TGA) were carried out dynamically applying a heating/cooling rate of 2 K min^{-1} in flowing (2 ml min^{-1}) air or oxygen streams to evaluate the oxygen stoichiometry stability of the samples from 298 K to 1173 K in an SDT Q600 thermogravimetric analyser.

In addition to the PXRD, the crystal structures of the materials were analysed by the combination of selected-area electron diffraction (SAED), high-resolution transmission electron microscopy (HRTEM), high-angle annular dark field (HAADF) and annular bright field (ABF) scanning TEM (STEM) and electron energy-loss spectroscopy (EELS). For TEM studies, the compounds were ground in *n*-butyl alcohol and ultrasonically dispersed. A few drops of the resulting suspension were deposited on a carbon-coated grid. SAED, HRTEM and EELS experiments were performed with a JEOL JEM 3000F microscope operating at 300 kV (double tilt $\pm 20^\circ$) (point resolution 0.17 nm), and fitted with a X-ray energy dispersive spectroscopy (XEDS) microanalysis system (OXFORD INCA) and an ENFINA spectrometer with an energy resolution of 1.3 eV. The atomic ratio of the metals was determined by XEDS analysis finding good agreement between analytical and nominal composition in all the crystals. The average oxidation state of Mn atoms of the oxide was determined by EELS.[26] When necessary, plural-scattering effects were removed with a Fourier-ratio deconvolution method.[26] The spectra were acquired in diffraction mode, with a dispersion of 0.1 eV per channel, a collection angle $\beta \sim$ 5.3 mrad and an acquisition time of 2 s. The HAADF and ABF STEM experiments and EELS mapping were performed on an ARM200cF microscope, fitted with a condenser lens aberration corrector (point resolution in STEM mode of 0.08 nm) and a GIF Quantum-ER spectrometer. HAADF images were acquired with an inner acceptance angle of 90 mrad and ABF ones with a collection angle of 11 mrad. EELS mapping was performed with a collection semi-angle $\beta \sim 30$ mrad, 0.5 eV per channel dispersion and a collection time for each spectrum of 0.09 seconds. Gd-$M_{4,5}$, Ba-$M_{4,5}$, Co-$L_{2,3}$ and Mn-$L_{2,3}$ edge signals were chosen for mapping.

The electrical characterization was performed by d.c. four probe methodology. 99% densified rectangular bars were prepared by sintering at 1473 or 1773 K (depending on the composition) and four electrodes were prepared by attaching Pt

wires with Pt paste and firing at 1223 K for 1 hour. Potentiostat/galvanostat (Autolab PGStat302N) equipment was employed to produce the current flow through the sample by means of the external electrodes and also to read the voltage difference between the inner electrodes. The resistances of the samples were determined from the slopes of the linear *I–V* curves in the temperature range of 423–1223 K.

Area specific resistance (ASR) values associated with the electrode polarization processes in air were determined from complex impedance spectra obtained by AC impedance spectroscopy on symmetrical two-electrode configuration cells at different temperatures. The high-frequency offset in the impedance spectra is associated with the electrolyte resistance, whereas the difference between the high and low frequency intercepts on the real axis (Z') is associated with all the resistive processes taking place at the electrodes. Electrolyte pellets of 10 mm diameter and 1.2 mm thickness of commercial $Ce_{0.9}Gd_{0.1}O_{2-\delta}$ (CGO) powder (fuel cells materials) were prepared with 99% density by pressing the powder at 250 MPa and sintering in air at 1673 K for 12 hours. Slurries prepared using $GdBaCo_{2-x}Mn_xO_{5+\delta}$: CGO composites (70 : 30 wt%) with a commercial organic vehicle (Decoflux™) were deposited onto both surfaces of the CGO electrolyte pellets and then fired at 1173 K for 3 h in air (heating/cooling rate of 2.5 K min^{-1}). The experimental procedure was carefully followed by SEM for the preparation of different systems in order to minimize microstructural differences and corresponding effects on the later electrochemical behavior. Silver paste and mesh were used as current collectors on both sides of the pellets. The impedance measurements were carried out using a frequency response analyzer Solartron 1255A with a dielectric interface 1296. Measurements were performed in air on heating and cooling cycles between 723 K and 923 K, in a frequency range of 0.1 Hz to 1 MHz and an excitation voltage of 50 mV.

Results and discussion

Fig. 1 shows the PXRD patterns of $GdBaCo_{2-x}Mn_xO_{5+\delta}$ with $x = 0.2$ and 1.8 synthesised in air. The pattern of $GdBaCo_{1.8}Mn_{0.2}O_{5+\delta}$ is indexed using tetragonal S.G. *P4/mmm* and unit cell $a_p \times a_p \times 2a_p$ (a_p refers to the lattice parameter of the cubic perovskite). In contrast, the pattern of $GdBaCo_{0.2}Mn_{1.8}O_{5+\delta}$ is indexed as a cubic disordered perovskite (S.G. *Pm3m*; $Gd_{0.5}Ba_{0.5}Co_{0.1}Mn_{0.9}O_{2.5+\delta}$). The patterns of all the compounds prepared in argon are similar to that of $GdBaCo_{1.8}Mn_{0.2}O_{5+\delta}$ in Fig. 1a. The PXRD results indicate that, under an argon atmosphere, single-phase samples can be obtained for the whole compositional range, $GdBaCo_{2-x}Mn_xO_{5+\delta}$ ($0 \leq x \leq 2$), whereas in air the $x = 0$ member cannot be prepared; thus, single-phase $GdBaCo_2O_{5+\delta}$ is only obtained in an argon atmosphere.[3] Layered-type ordered perovskites, with tetragonal symmetry S.G. *P4/mmm* and unit cell $a_p \times a_p \times 2a_p$, are obtained when the synthesis proceeds in argon flow for the whole compositional range. However, when the materials are prepared in air, ordering of Ba and Gd only occurs for compositions in the range $0 < x < 1.4$ (for $x > 1.4$, cubic disordered perovskites with S.G. *Pm3m* are obtained). The compositional range of ordered oxides is wider than that observed in the analogous Nd-system,[15–17] probably due to the larger size difference between Gd and Ba in comparison to Nd and Ba.

The thermal stability of the materials was studied by TGA (Fig. S1, ESI†). Table 1 collects the δ values of different oxides after preparation and after the first heating/cooling cycle. Although the materials prepared in Ar have slightly lower oxygen content after the first heating–cooling cycle, the oxygen content does not seem to strongly depend on the conditions of synthesis, unlike the crystal structure. The oxygen content in $GdBaCo_{2-x}Mn_xO_{5+\delta}$ increases as the substitution of Mn for Co increases. The air-prepared oxides suffer significant oxidation

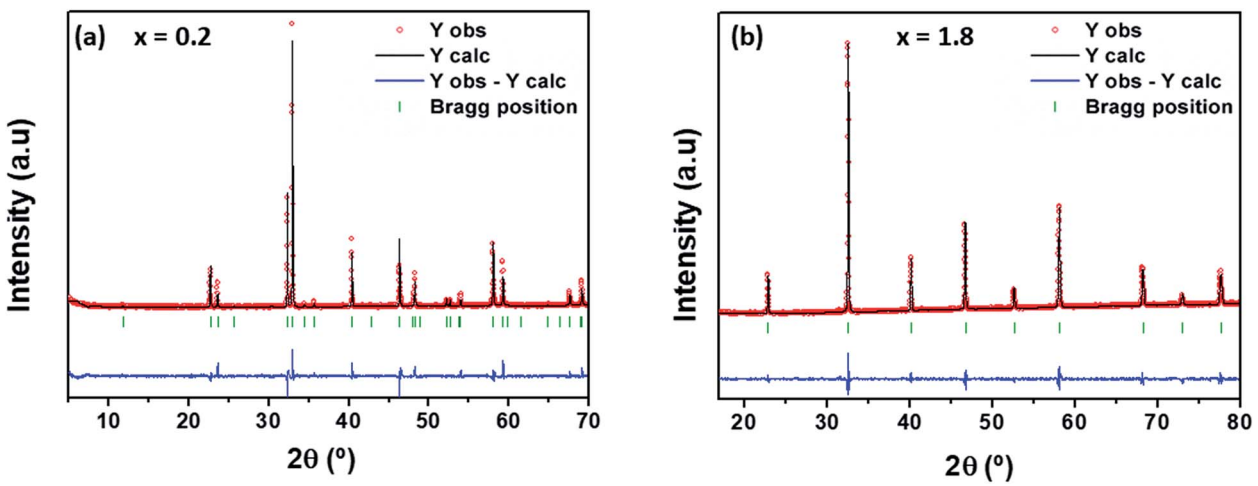

Fig. 1 Room temperature PXRD patterns (red points) of two oxides of the $GdBaCo_{2-x}Mn_xO_{5+\delta}$ system prepared in air, $x = 0.2$ (a) and $x = 1.8$ (b). Profile fitting has been carried out with (a) the *P4/mmm* space group and $a_p \times a_p \times 2a_p$ unit cell and (b) the *Pm3m* space group and $a_p \times a_p \times a_p$ unit cell. Calculated patterns correspond to the black line, and their difference with the experimental ones is indicated in blue at the bottom of each panel.

Table 1 Oxygen content (given as δ values in the general formula $GdBaCo_{2-x}Mn_xO_{5+\delta}$) obtained for the as-prepared samples (from redox titration) and during heating–cooling processes in air for different values of x in the $GdBaCo_{2-x}Mn_xO_{5+\delta}$ system prepared in air and argon

	Samples prepared in air			Samples prepared in argon		
Composition	δ (RT) as prepared	δ (1173 K)	δ (RT) after the heating/cooling cycles	δ (RT) as prepared	δ (1173 K)	δ (RT) after the heating/cooling cycles
$GdBaCo_{1.8}Mn_{0.2}O_{5+\delta}$	0.10(2)	0.27	0.48	0.12(2)	0.18	0.45
$GdBaCo_{1.4}Mn_{0.6}O_{5+\delta}$	0.22(4)	0.35	0.56	0.20(4)	0.20	0.48
$GdBaCoMnO_{5+\delta}$	0.39(2)	0.53	0.80	0.40(4)	0.41	0.68
$GdBaCo_{0.6}Mn_{1.4}O_{5+\delta}$	0.57(4)	0.80	1.00	0.64(4)	0.70	0.87
$GdBaCo_{0.2}Mn_{1.8}O_{5+\delta}$	0.76(3)	0.85	0.96	0.74(4)	0.70	0.75
$GdBaMn_2O_{5+\delta}$	0.85(3)	0.92	0.95	0.75(3)	0.60	0.75

on heating from room temperature up to about 723 K; above 723 K, the loss of oxygen occurs (Fig. S1a, b†). On cooling, the materials oxidise but the second heating–cooling cycle is reversible and consists of only two processes (loss of oxygen on heating above 723 K and uptake of oxygen on cooling). The oxidation of the compounds during the initial heating is probably related to the instability of the as-prepared phase due to the fast cooling on preparation and it also occurs in the $NdBaCo_{2-x}Mn_xO_{5+\delta}$ oxides.[3,15] The oxides prepared in argon show lower variations of oxygen content on heating–cooling cycles (Table 1 and Fig. S1c, d†). It is noteworthy that variations of the oxygen content with temperature are clearly lower with increasing the Mn content. This agrees with previous results reported in systems such as $Nd_{0.6}Sr_{0.4}Co_{1-y}Mn_yO_{3-\delta}$ [27] or $NdBaCo_{2-x}Mn_xO_{5+\delta}$ [15] and suggests a stronger binding of oxygen in oxides with higher Mn contents.

Therefore, the sample without cobalt presents a very stable value of δ as a function of temperature after the first heating/cooling cycle (Fig. S1 b, d†), indicating a very stable value of the average oxidation state of Mn. This behaviour suggests that the changes in the oxygen content of Mn–Co-based samples during heating/cooling processes are mainly related to variations in the oxidation state of Co.

Fig. 2 shows the TEC values of the oxides of the $GdBaCo_{2-x}Mn_xO_{5+\delta}$ system calculated in the range of temperatures 575 K < T < 1200 K. TEC values were determined from the variation of their unit cell volume with temperature (Fig. S2†) and unit cell volumes were determined from the PXRD patterns taken from room temperature up to 1173 K (Fig. S3†). TEC values significantly decrease with increasing the Mn content as a result of two effects: decreasing the oxygen loss with temperature and lower concentration of Co^{3+} which diminishes the effect associated with the spin state transition. Similar variation of TEC values is observed in other systems such as $NdBaCo_{2-x}Mn_xO_{5+\delta}$ (ref. 15) and $SmSrCo_{2-x}Mn_xO_{5+\delta}$.[28]

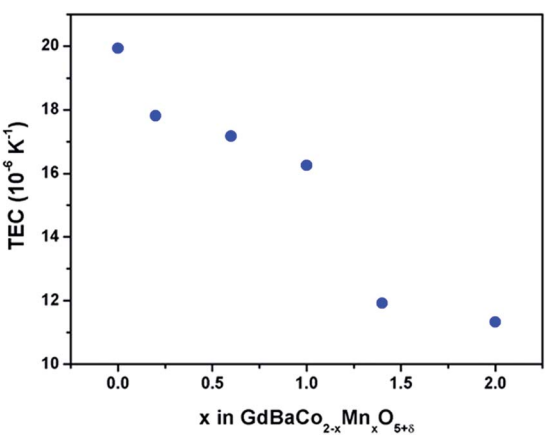

Fig. 2 TEC values of the oxides of the $GdBaCo_{2-x}Mn_xO_{5+\delta}$ system calculated in the range of temperatures 575 K < T < 1200 K.

The crystal structure of the $GdBaCo_{2-x}Mn_xO_{5+\delta}$ oxides has been confirmed by SAED and HRTEM (Fig. S4†). The SAED patterns and corresponding HRTEM images of the compounds with $0 \leq x < 2$ prepared in argon and the compounds with $0 < x < 1.4$ prepared in air are characteristic of layered-type perovskites.[3,12] In $GdBaMn_2O_{5.75}$, modulation of the crystal structure due to Mn^{3+}/Mn^{4+} charge ordering has been reported.[29] The results of the materials prepared in air with composition corresponding to $1.4 \leq x \leq 2$ are characteristic of the perovskite structure, as no ordering of Gd and Ba atoms occurs. A more detailed study of the crystal structure of $GdBaCoMnO_{5+\delta}$ has been carried out by means of STEM and EELS in order to confirm the Ba and Gd ordering and to determine the location of the Co and Mn atoms and the anion vacancies. Fig. 3 displays the HAADF-STEM image and corresponding FFT along the $[100]_p$ zone axis, intensity line profiles and EELS mapping. The FFT of the image indicates a modulation of the crystal structure of the cubic perovskite along the $[001]_p$ direction corresponding to $c \sim 2a_p$.

The contrast differences observed in the image, in agreement with the modulation and confirmed by the intensity line profile run along $[001]_p$ on a row of columns of A-type atoms (Ba and Gd), indicate layered-type ordering of cations. The EELS mapping demonstrates that Gd and Ba are distributed in the alternating $(001)_p$-layers and that Co and Mn are located randomly within the B positions of the perovskite-type structure. When the line intensity profile is taken on columns of Co/Mn atoms along the $[001]_p$ direction, two alternating distances (0.34 nm and 0.42 nm) between these atoms are detected. The displacement of consecutive Co/Mn atoms towards the Gd–O layers causes the alternation of these two Co/Mn–Co/Mn distances. Therefore, a combination of both compositional

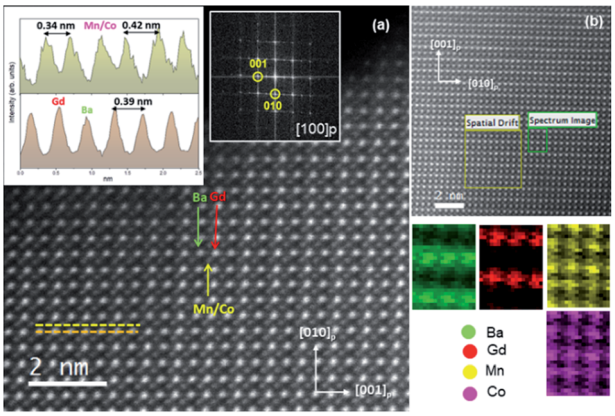

Fig. 3 (a) HAADF-STEM image of a $GdBaCoMnO_{5+\delta}$ crystal along the $[100]_p$ orientation. The corresponding FFT is included as an inset. The intensity line-profiles along the Gd/Ba (orange line on the image) and along the Mn/Co (yellow line on the image) positions are displayed on the left top corner. (b) EELS maps from a crystal along the $[100]_p$ orientation.

and displace-type two-fold modulations of the crystal structure occurs along the $[001]_p$ direction.

Fig. 4 shows the ABF and HAADF-STEM images of the $[100]_p$ zone axis for comparison. The intensity line profile running along $[001]_p$ on the rows of Gd/O/Ba/O columns in the BF image reveals two alternating Gd–O/Ba–O distances. Oxygen atoms are drawn closer to the Gd positions (0.17 nm) than to the Ba positions (0.21 nm). Moreover, the intensity profile along (CoMn)/O columns indicates a lower concentration of oxygen atoms in the Gd–O layers. This agrees with a lower contrast at the anion sites of the Gd–O layers. Therefore, we confirm that the anion vacancies are located at the Gd–O layers.

Fig. 5 shows the temperature dependence of the d.c. conductivity of different oxides of the $GdBaCo_{2-x}Mn_xO_{5+\delta}$ system prepared in air. The samples were heated at 1173 K for 12 h to equilibrate the oxygen content before starting the measurements on cooling.

The electrical behavior and conductivity values of the materials prepared in Ar are similar to those of the oxides with the same composition but prepared in air. For the compounds with $x = 0.2$ and 0.6, the conductivity increases with temperature up to ~723–773 K and then decreases, as it is expected because of the p-type electronic character of these materials (Fig. S5†) and the loss of oxygen above 723 K (loss of electron hole species when the oxygen vacancy content increases). However, the oxides with $x \geq 1$ present a different electrical behavior: the conductivity continuously increases with temperature and a decrease is not detected despite the fact that oxygen losses also occur above 723 K. Similar trends have previously been observed for $SmSrCo_{2-x}Mn_xO_{5+\delta}$ [28] and $NdBaCo_{2-x}Mn_xO_{5+\delta}$,[15] suggesting a change in the conduction mechanism by substituting Mn for Co. Moreover, comparison of the conductivity values at a fixed temperature with the Mn content (Fig. 6 at 923 K) indicates that the substitution of Co with Mn produces a monotonous decrease of conductivity for contents of Mn corresponding to $x \leq 1.2$ followed by a slight increase of conductivity for higher contents of Mn, which is also consistent with a change in the conduction mechanism. This variation of the conductivity with the composition seems to be characteristic of the Co/Mn systems.[15,30]

The electrical properties of $GdBaCo_{2-x}Mn_xO_{5+\delta}$ might be associated with a polaron hopping mechanism ascribed to electron hole transfer between $(Co,Mn)^{4+}$ and $(Co,Mn)^{3+}$ sites. It has been previously outlined that there exists a preferential electrical compensation by the formation of Mn^{4+} instead of the formation of Co^{4+}, which also coexists with different degrees of oxygen vacancies depending on the level of doping.[27,28,30]

When small contents of Mn ($x = 0.2$) are introduced by substitution of the Co species, the main oxidation state of Mn is close to 4+ according to our EELS results. Given that the amount of Mn^{3+} is very low because of the lower contents of Mn, the

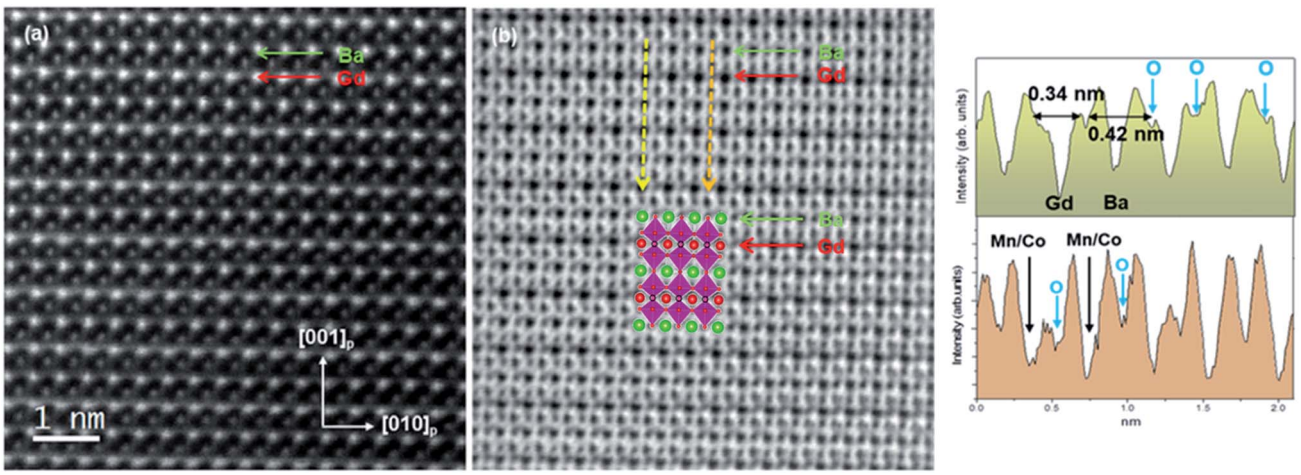

Fig. 4 (a) HAADF-STEM and (b) ABF-STEM images of a $GdBaCoMnO_{5+\delta}$ crystal along the $[100]_p$ orientation. The intensity line-profile (top right) along the $[001]_p$ direction on the Ba/O/Gd/O positions (yellow line on the ABF image) reveals that oxygen columns are closer to Gd than to Ba. The intensity line profile on the (CoMn)/O positions (orange line on the ABF image) suggests that oxygen vacancies are concentrated in the Gd–O layers. The columns of oxygen atoms containing these vacancies, within the Gd–O planes, are indicated by filled circles.

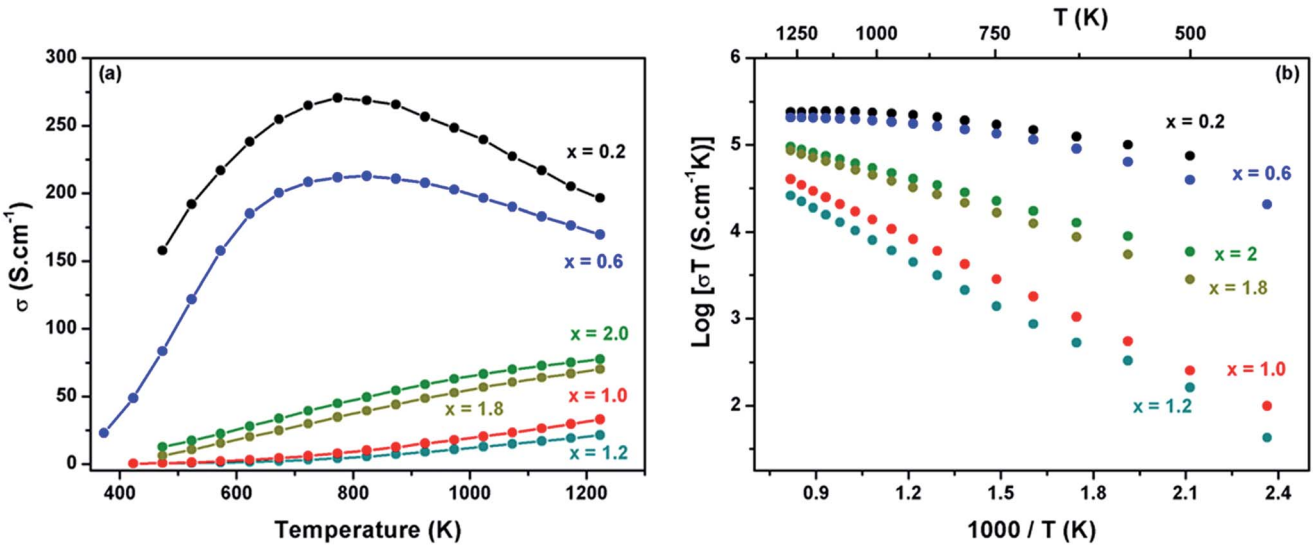

Fig. 5 (a) Temperature dependence of conductivity measured in air and (b) Arrhenius representation of the total conductivity measured in air of $GdBaCo_{2-x}Mn_xO_{5+\delta}$ oxides with $x = 0.2$, 0.6, 1.0, 1.2, 1.8 and 2.0 prepared in air.

electrical conduction may occur mainly by adjacent Co^{4+}/Co^{3+} sites and the Mn^{4+} ions have the effect of acting as hole traps, decreasing the electronic conductivity in comparison to $BaGdCo_2O_{5+\delta}$.

Kostogloudis *et al.*[30] reported that the transition rate between two adjacent cobalt sites is higher than that between two adjacent manganese sites, which implies that cobalt sites are the preferred movement for holes, producing high values of conductivity and low activation energies for low contents of Mn.

Therefore, an increase in the Mn content produces a decrease of the electrical conductivity by a simple decrease of the concentration of the dominating conducting species. At this point, it is worth mentioning that in $GdBaMn_2O_{5+\delta}$, the average oxidation state of Mn was reported to be 3.28, which confirmed that the material has Mn^{4+}/Mn^{3+} species.[28]

Taking into account that Mn^{4+} is more stable than Co^{4+}, reduction of Co^{4+} to Co^{3+} is expected when Co is substituted with Mn in this system, eliminating Co^{4+}/Co^{3+} pairs. Therefore, a high Mn concentration produces enough content of Mn^{3+} for the movement of the electron holes to take place through adjacent Mn sites, given that the transition rate for Mn^{4+}/Mn^{3+} sites is considerably higher than that of Mn^{4+}/Co^{3+} sites.[30] Once the dominant conduction-mechanism consists of polaron-hopping between Mn^{4+} and Mn^{3+} sites ($x > 1$), the conductivity increases with increasing the amount of Mn^{4+}/Mn^{3+} species. It is important to note that the loss of oxygen in samples with $x \geq 1$ for $T > 723$ K is not expected to produce a decrease of the concentration of active holes for the electrical conduction. The oxidation states of Mn are generally very stable with temperature, suggesting that the oxygen loss may be associated with changes in the oxidation state of Co species. As a consequence, the concentration of electronic-conducting species, associated with Mn^{4+}/Mn^{3+} pairs, should not be considerably affected by temperature, which is consistent with the behaviour observed for the samples with higher contents of Mn (Fig. 6).

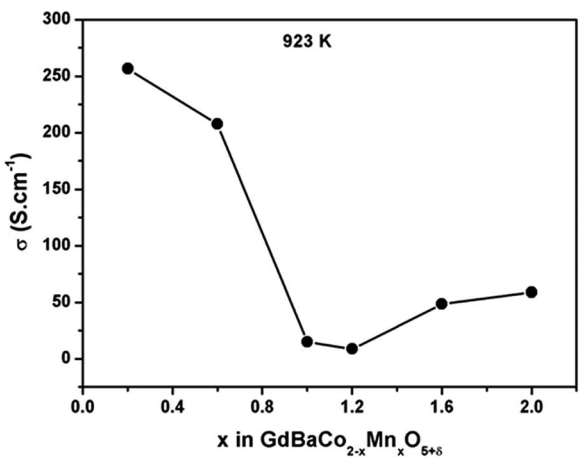

Fig. 6 Variation of conductivity measured in air for $GdBaCo_{2-x}Mn_xO_{5+\delta}$ as a function of manganese content (x) at 923 K.

The chemical compatibility of the oxides with the electrolyte (CGO) was determined prior to the study of their electrochemical properties in symmetrical cells. The PXRD patterns of the $GdBaCo_{2-x}Mn_xO_{5+\delta}$: CGO (70 : 30 wt%) composites heated at 1173 K for 12 hours only show reflections corresponding to the material under study and CGO (Fig. S6† shows one example), suggesting that either the reaction between these two compounds does not occur or the fraction of the new phase(s) is below the detection limit of XRD. The electrolyte/electrode quality of contact, in addition to the possible formation of new phases in the surface of the contact between components of the symmetrical cell, was also evaluated by scanning electron microscopy (SEM). Fig. S7† shows a scanning electron microscopy (SEM) image of a cross-section of one of the cells after impedance measurements, which confirms a good adhesion between the electrode and electrolyte without apparent

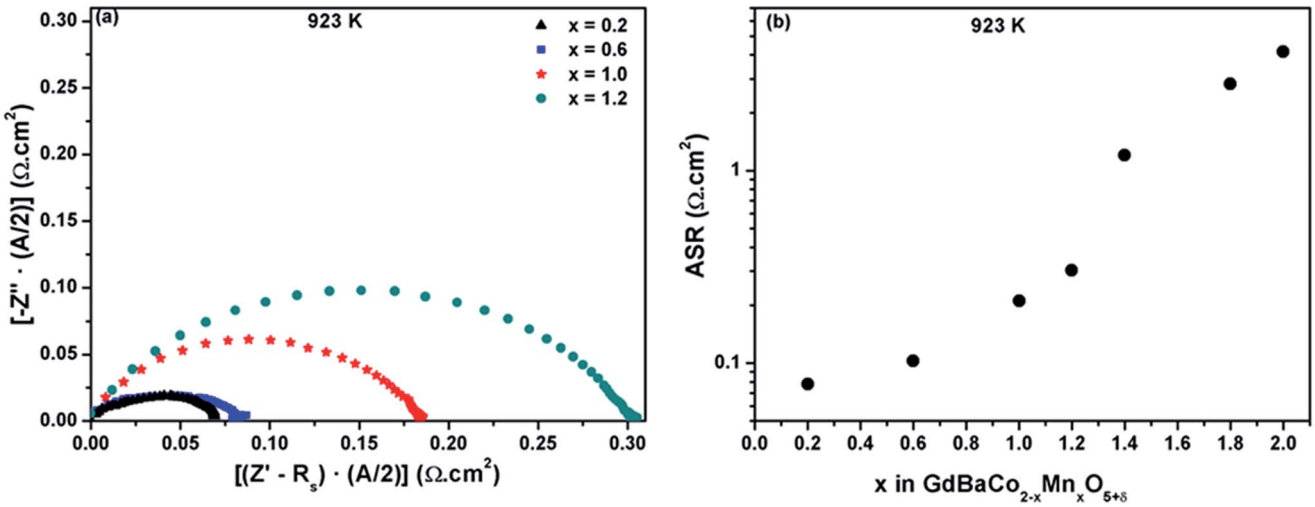

Fig. 7 (a) Impedance spectra of symmetrical cells using $GdBaCo_{2-x}Mn_xO_{5+\delta}$ prepared in air with $x = 0.2$, 0.6, 1.0 and 1.2. (b) Variation of ASR values for $GdBaCo_{2-x}Mn_xO_{5+\delta}$ prepared in air as a function of manganese content at 923 K.

interdiffusion between the components. A homogeneous distribution of CGO and GBCM as cathode-composite constituents is also observed.

The electrochemical behavior of the $GdBaCo_{2-x}Mn_xO_{5+\delta}$ oxides prepared either in air or in argon was evaluated by complex impedance spectroscopy measurements in symmetrical cells using these materials as the electrodes, as it is explained in the Experimental section. Fig. 7a shows impedance diagrams at 923 K of cells using different materials prepared in air as electrodes. The spectra were displaced to the origin of the Z' axis in order to remove the ohmic contribution and to compare different electrode processes.

As a general aspect, the electrode performance is affected as the Mn content increases, which agrees well with the results previously reported for relative Co/Mn systems.[15,28,31,32] The area-specific-electrode-polarization resistance (ASR) is clearly lower for the samples with lower contents of Mn, $x \leq 0.6$ (Fig. 7b), corresponding to samples with higher electronic conductivity (Fig. 5) and lower oxygen content (Table 1). It is important to note that the decrease of the electronic conductivity by more than one order of magnitude for $x = 1$ in comparison to $x = 0.6$ only produces the deterioration of the electrode performance by a factor of 2, which points to the oxygen vacancy concentration as the key factor for the oxygen electrochemical reaction. For higher Mn contents ($x \geq 1.4$), the ASR increases (Fig. 7b), despite having similar or even higher values of electronic conductivities. Table 1 shows that these compositions possess low oxygen deficiency, which diminishes as the Mn concentration increases, concomitant with the increase of ASR, supporting that the oxygen content might be the dominant factor in the electrode performance.

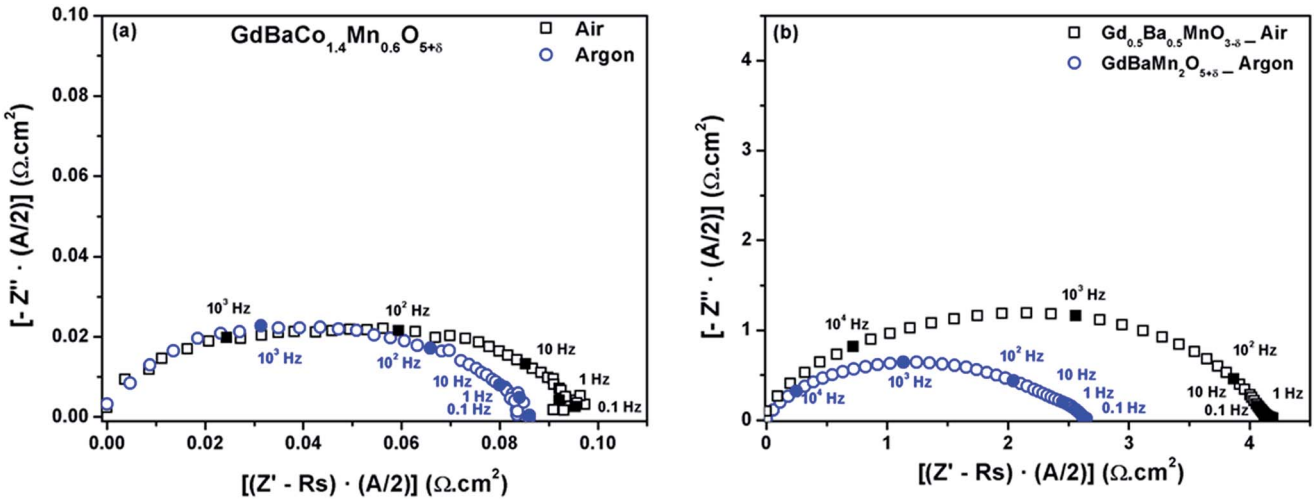

Fig. 8 Impedance spectra of symmetrical cells $GdBaCo_{2-x}Mn_xO_{5+\delta}$: CGO/CGO/$GdBaCo_{2-x}Mn_xO_{5+\delta}$: CGO at 923 K in air. (a) $x = 0.6$ prepared in air and argon; (b) $x = 2.0$ prepared in air and argon.

Table 2 ASR values at 923 K of symmetrical cells with different oxides of the $GdBaCo_{2-x}Mn_xO_{5+\delta}$ system prepared in air and argon

	ASR (Ω cm^2) at 923 K	
Composition	Samples prepared in air	Samples prepared in argon
$GdBaCo_{1.8}Mn_{0.2}O_{5+\delta}$	0.078	0.075
$GdBaCo_{1.4}Mn_{0.6}O_{5+\delta}$	0.095	0.082
$GdBaCoMnO_{5+\delta}$	0.210	0.187
$GdBaCo_{0.6}Mn_{1.4}O_{5+\delta}$	1.10	1.09
$GdBaCo_{0.2}Mn_{1.8}O_{5+\delta}$	2.65	1.36
$GdBaMn_2O_{5+\delta}$	4.13	2.89

Fig. 8a and b show impedance diagrams at 923 K of cells assembled with electrodes corresponding to $GdBaCo_{2-x}Mn_xO_{5+\delta}$ oxides ($x = 0$,6 and 2.0) prepared either in air or in argon. For low contents of Mn, the samples have similar ASR values independent of the synthesis conditions of the material; however, for high Mn contents, the compositions prepared in argon show lower ASR values than those corresponding to compositions prepared in air. Taking into account that all the compositions prepared in argon present ordering of Gd and Ba cations in the crystal structure, which only exists for $0 < x < 1.4$ in the samples prepared in air, these results demonstrate that the cells with electrodes using oxides presenting cation ordering have similar ASR values not depending on the synthesis conditions of the material. However, the cells using layered-perovskites in the electrodes present significantly lower ASR values than those using compounds of the same composition but with the Ba and Gd atoms statistically distributed within the structure.

Therefore, the $GdBaCo_{2-x}Mn_xO_{5+\delta}$ system seems to be a new example of experimental evidence of the better electrochemical properties of layered-perovskites compared to those of perovskites with random location of the A-cations and therefore random location of the oxygen vacancies. Table 2 summarizes the ASR values of all the cells measured at 923 K. Values lower than 0.15 Ω cm^2 are found for cells with electrodes using $GdBaCo_{2-x}Mn_xO_{5+\delta}$ oxides with $x < 1.0$, indicating good behavior of these materials as air-electrodes in IT-SOFCs, although optimization of the cell construction is essential for the application of the materials.

Conclusions

Materials of the $GdBaCo_{2-x}Mn_xO_{5+\delta}$ ($0 \leq x \leq 2$) system have been synthesized under different conditions (in air or argon atmospheres) highly impacting the Gd/Ba cation ordering of the crystal structure. Layered-type ordering of Gd and Ba in the perovskite-type structure occurs in the whole range of composition of the system when the materials are prepared in argon, however, it occurs only for compositions corresponding to $x < 1.4$ when the materials are prepared in air. A 2-fold modulation associated with correlated displacements of consecutive Co/Mn atoms towards the Gd–O layers is observed in $GdBaCoMnO_{5+\delta}$ in addition to the layered cation-ordering.

These materials are p-type conductors and the d.c. conductivity results indicate a change in the conduction mechanism in the system from $x > 1$. The polaron hopping mechanism ascribed to electron hole transfer between M^{4+}/M^{3+} sites (M = Co, Mn) depends on the concentration of Co and Mn in the oxide. The conductivity decreases by the substitution of Mn for Co because the electron–hole transition rate is higher between Co^{4+}/Co^{3+} sites than that between Mn^{4+}/Mn^{3+} sites.

Electrochemical studies on symmetrical cells using these materials as electrodes reveal that the substitution of Mn for Co, in the $GdBaCo_{2-x}Mn_xO_{5+\delta}$ ($0 \leq x \leq 2$) system, increases the ASR values probably due to the decrease of the anion vacancies. In contrast, TEC values decrease with increasing the Mn content. Layered-type ordering of the Gd and Ba atoms seems to affect the electrochemical properties of these materials in such a way that materials with ordering show lower ASR values than those with a similar composition but with the A cations statistically distributed, which implies that the oxygen vacancies are also located randomly. Some of these oxides give ASR values lower than 0.15 Ω cm^2 at 923 K, indicating their promising good behaviour as air electrodes in IT-SOFCs by optimizing the cell.

Conflicts of interest

There are no conflicts to declare.

Acknowledgements

This work has been supported by MINECO with Projects MAT2013-46452-C4-4-R, MAT2016-78362-C4-1-R, MAT2016-78362-C4-4-R, ENE2015-66183-R and CM with project MATERYENER3CM-S2013/MIT-2753. U. A. also thanks the Universidad San Pablo for financial support. S. García-Martín thanks Prof. West for his unique teaching on solid state chemistry during her post-doc time at the University of Aberdeen.

References

1 A. Chang, S. J. Skinner and J. A. Kilner, *Solid State Ionics*, 2006, **177**, 2009–2011.
2 A. Tarancón, S. J. Skinner, R. J. Chater, F. Hernández-Ramírez and J. A. Kilner, *J. Mater. Chem.*, 2007, **17**, 3175–3181.
3 D. Muñoz-Gil, D. Pérez-Coll, J. Peña-Martínez and S. Garcia-Martín, *J. Power Sources*, 2014, **263**, 90–97.
4 A. A. Taskin, A. N. Lavrov and Y. Ando, *Prog. Solid State Chem.*, 2007, **35**, 481–490.
5 D. Parfitt, A. Chroneos, A. Tarancón and J. A. Kilner, *J. Mater. Chem.*, 2011, **21**, 2183–2186.
6 A. Tarancón, D. Marrero-López, J. Peña-Martínez, J. C. Ruiz-Morales and P. Núñez, *Solid State Ionics*, 2008, **179**, 611–618.
7 L. Mogni, F. Prado, C. Jiménez and A. Caneiro, *Solid State Ionics*, 2013, **240**, 19–28.
8 K. R. Zhdanov, M. Yu. Kameneva, L. P. Kozeeva and A. N. Lavrov, *Phys. Solid State*, 2010, **52**, 1688–1693.

9 S. Roy, M. Khan, Y. Q. Guo, J. Craig and N. Ali, *Phys. Rev. B: Condens. Matter Mater. Phys.*, 2002, **65**, 064437–064445.

10 R. Pelosato, G. Cordaro, D. Stucchi, C. Cristiani and G. Dotelli, *J. Power Sources*, 2015, **298**, 46–67.

11 B. Wei, Z. Lu, D. Jia, X. Huang, Y. Zhang and W. Su, *Int. J. Hydrogen Energy*, 2010, **35**, 3775–3782.

12 D. Muñoz-Gil, D. Pérez-Coll, E. Urones-Garrote, U. Amador and S. García-Martín, *J. Mater. Chem. A*, 2017, **5**, 12550–12556.

13 D. A. Medvedev, T. A. Zhuravleva, A. A. Murashkina, V. S. Sergeeva and B. D. Russ, *J. Phys. Chem.*, 2010, **84**, 1623–1627.

14 Y. N. Kim and A. Manthiran, *J. Electrochem. Soc.*, 2011, **158**, B276–B282.

15 T. Broux, M. Bahout, J. M. Hanlon, O. Hernandez, S. Paofai, A. Berenov and S. J. Skinner, *J. Mater. Chem. A*, 2014, **2**, 17015–17023.

16 O. L. Pineda, Z. L. Moreno, P. Roussel, K. Świerczek and G. H. Gauthier, *Solid State Ionics*, 2016, **288**, 61–67.

17 F. Tonus, M. Bahout, V. Dorcet, G. H. Gauthier, S. Paofai, R. I. Smith and S. J. Skinner, *J. Mater. Chem. A*, 2016, **4**, 11635–11647.

18 D. Muñoz-Gil, D. Ávila-Brande, E. Urones-Garrote and S. García-Martín, *Dalton Trans.*, 2015, **44**, 10867–10874.

19 S. García-Martín, K. Manabe, E. Urones-Garrote, D. Ávila-Brande, N. Ichikawa and Y. Shimakawa, *Inorg. Chem.*, 2017, **56**, 1412–1417.

20 S. Sengodan, S. Choi, A. Jun, T. Ho Shin, Y. W. Ju, H. Y. Jeong, J. Shin, J. T. S. Irvine and G. Kim, *Nat. Mater.*, 2015, **14**, 205–209.

21 T. H. Shin, J. H. Myung, M. Verbraeken, G. Kim and J. T. S. Irvine, *Faraday Discuss.*, 2015, **182**, 227–239.

22 Y. N. Kim and A. Manthiran, *J. Mater. Chem. A*, 2015, **3**, 24195–24210.

23 A. Le Bail, H. Duroy and J. L. Fourquet, *Mater. Res. Bull.*, 1988, **23**, 447–452.

24 J. Rodríguez-Carvajal, *Phys. B*, 1993, **192**, 55–69.

25 J. C. Pérez Flores, C. Ritter, D. Pérez-Coll, G. C. Mather, F. García-Alvarado and U. Amador, *J. Mater. Chem.*, 2011, **21**, 13195.

26 H. K. Schmid and W. Mader, *Micron*, 2006, **37**, 426–432.

27 K. T. Lee and A. Manthiram, *J. Power Sources*, 2006, **158**, 1202–1208.

28 Y. Wang, X. Zhao, S. Lü, X. Meng, Y. Zhang, B. Yu, X. Li, Y. Sui, J. Yang, C. Fu and Y. Ji, *Ceram. Int.*, 2014, **40**, 11343–11350.

29 D. Ávila-Brande, G. King, E. Urones-Garrote, S. Subakti, A. Llobet and S. García-Martín, *Adv. Funct. Mater.*, 2014, **24**, 2510–2517.

30 G. Ch. Kostogloudis, P. Fertis and Ch. Ftikos, *Solid State Ionics*, 1999, **118**(3–4), 241–249.

31 H. Lv, B.-Y. Zhao, Y.-J. Wu, G. Sun, G. Chen and K. Ao Hu, *Mater. Res. Bull.*, 2007, **42**, 1999–2012.

32 M. B. Phillipps, N. M. Sammes and O. Yamamoto, *Solid State Ionics*, 1999, **123**, 131–138.